# Elimination of Cross-Talk and Modulation of Function in an Organized Heterosupramolecular Assembly

**Alan Merrins, Xavier Marguerettaz, S. Nagaraja Rao, and Donald Fitzmaurice*[a]**

**Abstract:** A close-packed monolayer of $TiO_2$ nanocrystals was deposited on a conducting glass support using Langmuir–Blodgett (LB) techniques and fired. A close-packed mixed monolayer of eicosyl phosphonic acid (**I**) and the viologen, 1,1′-dieicosyl-4,4′-bipyridinium dichloride (**II**) was then deposited on the $TiO_2$ substrate, also using LB techniques. At sufficiently high dilutions of **II** in **I**, a single viologen molecule is adsorbed with a known orientation at the surface of each nanocrystal. The resulting assembly was incorporated as the working electrode in an electrochemical cell. Under open circuit conditions, bandgap excitation of a $TiO_2$ nanocrystal results in electron transfer to a viologen molecule. No electron transfer between the viologen molecules adsorbed at different nanocrystals is observed. At a positive applied potential, electron transfer following bandgap excitation is largely suppressed. Considered are the implications of these findings for the development of practical devices based on modulatable function addressable on the nanometer scale.

**Keywords:** bandgap excitation · electron transfer · nanostructures · supramolecular chemistry · titanium

## Introduction

A heterosupermolecule is formed by covalently and noncovalently linking condensed phase and molecular components.[1] By analogy with a supermolecule, the properties of the components of a heterosupermolecule largely persist and there exists an associated heterosupramolecular function.[2] Scheme 1 shows two heterosupermolecules formed by covalently and non-covalently linking a condensed phase ($TiO_2$ nanocrystal) and molecular (viologen) component, respectively.[3, 4] In each case the associated heterosupramolecular function, light-induced vectorial electron transfer, has been demonstrated.

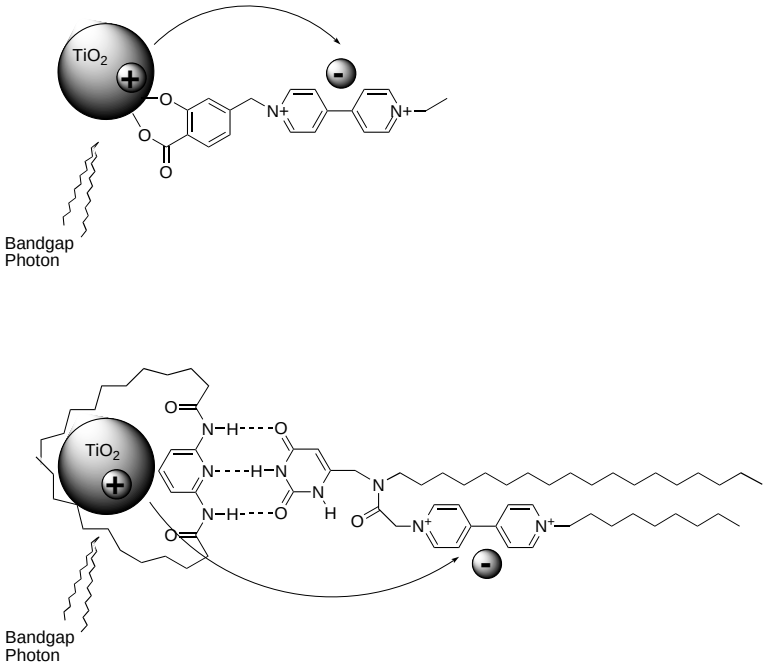


Scheme 1. Two examples of heterosupermolecules formed by covalently and noncovalently linking a condensed phase ($TiO_2$ nanocrystal) and molecular (viologen) component.

[a] Prof. D. Fitzmaurice, A. Merrins, X. Marguerettaz, S. N. Rao
Department of Chemistry
University College Dublin
Belfield, Dublin 4 (Ireland)
Fax: (+353) 1-706-2127
E-mail: donald.fitzmaurice@ucd.ie

The heterosupramolecular assembly shown in Scheme 2 was prepared by chemisorbing molecular components (viologen) at the surface of the constituent condensed phase components ($TiO_2$ nanocrystal) of a nanostructured film. The above heterosupramolecular assembly was incorporated as

  0947-6539/01/0706-1309 $ 17.50+.50/0 

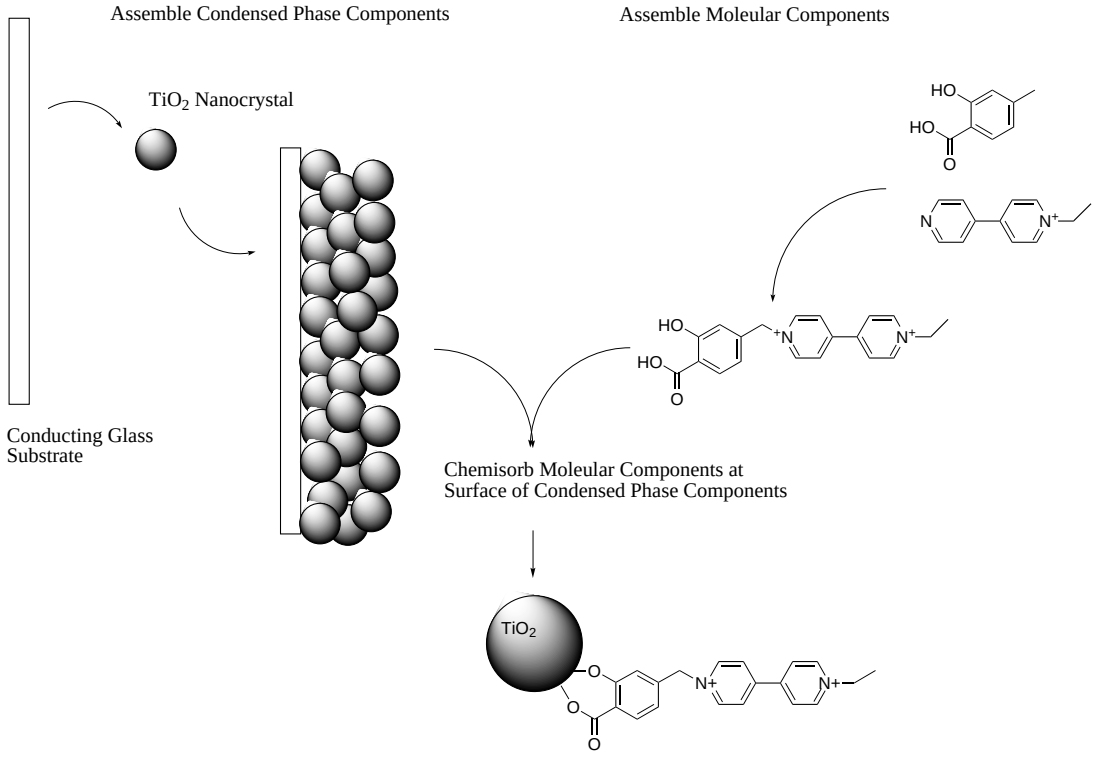


Scheme 2. Formation of a heterosupramolecular assembly.

the working electrode in an electrochemical cell. Under open circuit conditions, bandgap excitation results in electron transfer to the viologen. At positive applied potentials electron transfer is largely suppressed.[5] Function modulation is effective because each $TiO_2$ nanocrystal is simultaneously a component of a heterosupermolecule and of the nanostructured film used to effect function modulation. The nanostructured film is termed an *intrinsic substrate*.

The heterosupramolecular assembly in Scheme 2 has the following limitations:[5] Firstly, the heterosupermolecules cannot be addressed individually, as the location of a given heterosupermolecule within the assembly is not uniquely determined; secondly, the heterosupermolecules do not act independently, a consequence of electron transfer between the components of adjacent heterosupermolecules; and thirdly, the mechanism by which function modulation is effected is poorly understood, mainly because the properties of nanostructured semiconductor electrodes are themselves poorly understood.

To begin to address these limitations, an organised heterosupramolecular assembly has been prepared. Briefly, a close-packed monolayer of $TiO_2$ nanocrystals was deposited on conducting glass using Langmuir-Blodgett (LB) techniques and fired. A close-packed mixed monolayer of eicosyl phosphonic acid (**I**) and the viologen 1,1′-dieicosyl-4,4′-bipyridinium dichloride (**II**) was then deposited on the $TiO_2$ substrate, also using LB techniques. At sufficiently high dilutions of **II** in **I**, a single viologen molecule is adsorbed with a known orientation at the surface of each nanocrystal. The resulting assembly was incorporated as the working electrode in an electrochemical cell and electron transfer to the viologen, following bandgap excitation of a $TiO_2$ nanocrystal, monitored under open circuit conditions and at a positive applied potential.

It was expected that for the organised heterosupramolecular assembly described above the following would be the case: Firstly, that each heterosupermolecule would be individually addressable; secondly, that each heterosupermolecule would act independently within the assembly; and thirdly, that function modulation would be effective and accounted for by a well defined mechanism. Herein we consider the extent to which these expectations have been met and the consequent implications for the development of practical devices based on modulatable function addressable on the nanometer scale.

## Results and Discussion

### Deposition and characterisation of close-packed monolayers of $TiO_2$ nanocrystals on a conducting glass support

A heat-treated $TiO_2$ (anatase) sol, stabilised by cetyltrimethylammonium bromide (CTAB), was prepared following the method of Kotov et al.[6] The constituent nanocrystals, characterised by optical absorption spectroscopy and transmission electron microscopy (TEM), possess an absorption onset at $370 \pm 10$ nm and an average diameter of $23 \pm 2$ Å.[6, 7] Use of CTAB as a stabiliser ensures these nanocrystals are hydrophobic, form a monolayer on water and may be deposited on a suitable substrate using LB techniques.[8] By adopting this approach, a monolayer of $TiO_2$ nanocrystals has been deposited on a carbon coated nickel grid and fired at 450 °C for 2 h. From the corresponding TEM (Figure 3b of reference [8a]) it is clear that the deposited nanocrystals are close-



0947-6539/01/0706-1310 $ 17.50+.50/0 *Chem. Eur. J.* **2001**, *7*, No. 6

packed despite, as a consequence of the initially adsorbed CTAB layer, being separated by 3 Å.

Up to ten monolayers of $TiO_2$ nanocrystals have been deposited on fluorine-doped tin oxide glass.[8] Firing at 450 °C for 2 h removes the adsorbed CTAB and forms an ohmic contact (see below) between the deposited nanocrystals and the conducting glass support. Figure 1 shows the optical

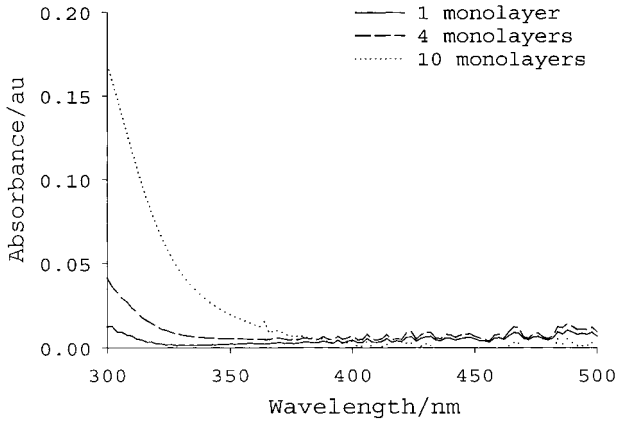


Figure 1. Optical absorption spectra of indicated number of close-packed monolayers of $TiO_2$ nanocrystals deposited on a microscope slide and fired for 2 h at 450 °C.

absorption spectra of one, four and ten monolayers of $TiO_2$ nanocrystals deposited on a standard microscope slide and fired in air at 450 °C for 2 h. Microscope slides are used in this instance because the resulting spectra, due to the absence of interference fringes caused by the metal oxide film present on conducting glass, are of superior quality. As expected, the measured absorbance increases linearly with the number of deposited monolayers.

It has been observed, in the case of a nanostructured $TiO_2$ (4 μm thick) film deposited on conducting glass, that electrons occupy available states of the conduction band at applied potentials more negative than the potential of the conduction band edge ($V_{cb}$) at the semiconductor–liquid electrolyte interface (SLI). Occupation of the available conduction band states is accompanied by an absorbance increase at wavelengths longer than that corresponding to the onset of bandgap excitation.[9] This absorbance increase is accounted for by Drude theory modified for electron scattering in a semiconductor lattice by phonons and ionised impurities.[9, 10] Occupation of the available conduction band states is also accompanied by an absorbance decrease at wavelengths shorter than that corresponding to the onset of bandgap excitation.[9] This absorbance decrease is accounted for by the Burstein–Moss shift that accompanies band-filling.[9, 11]

Figure 2a shows the potential-dependent optical absorption spectra measured at pH 2.0 for a monolayer of $TiO_2$ nanocrystals deposited on conducting glass. The absorbance changes observed at applied potentials more negative than $V_{cb}$ are assigned to the Burstein–Moss shift and the Drude absorption accompanying occupation of available conduction band states by electrons.[9, 11] Similar spectra are measured at pH 12.0 although, the absorbance changes observed at a given applied potential are smaller than those measured at pH 2.0.

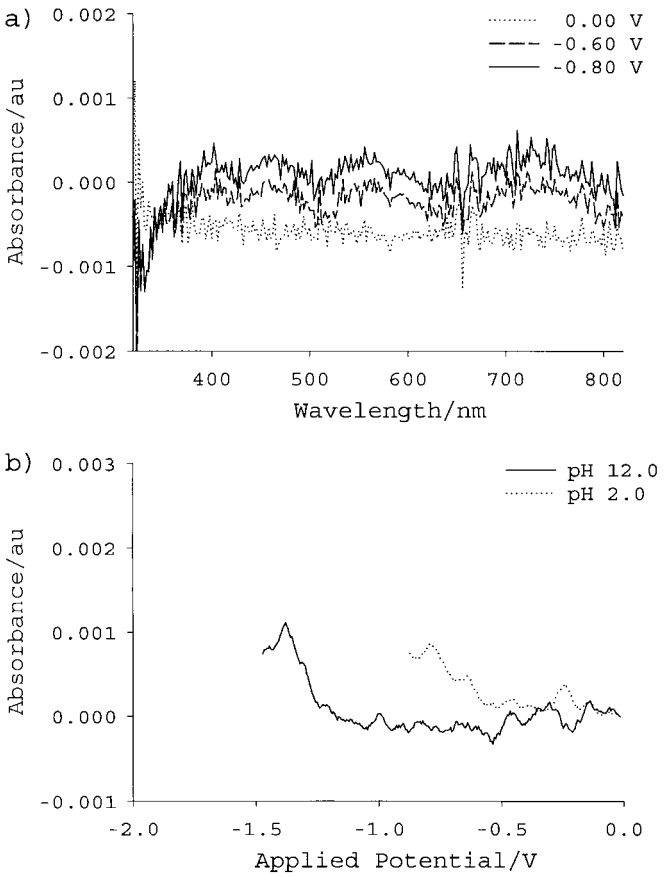


Figure 2. a) Potential-dependent optical absorption spectra of a close-packed monolayer of $TiO_2$ nanocrystals deposited on F-doped tin oxide glass and fired for 2 h at 450 °C. Spectra were measured at the indicated pH and applied potentials versus SCE against a background spectrum measured at 0.00 V. b) Absorbance increase at 780 nm of sample in a). Absorbance changes were measured at the indicated pH and applied potentials versus SCE against a background measured at 0.00 V.

Figure 2b shows the absorbance increases at 780 nm at pH values of 2.0 and 12.0 observed on sweeping the applied potential to more negative values. Clearly, electrons occupy the available conduction band states at more negative potentials at pH 12.0. This observation is consistent with a shift of the conduction band edge to more negative potentials at higher pH values, a property characteristic of metal oxide semiconductors in aqueous solution.[12, 13] The measured shift in the onset for absorption of 60 mV/pH unit is close to the expected value.[12, 13] Consequently, the measured onset for absorption has been used to estimate $V_{cb}$. It is also noted that the values obtained, –0.6 V and –1.2 V at pH 2.0 and pH 12.0, respectively, are in good agreement with those determined previously for nanoporous-nanocrystalline films prepared either by LB or sol–gel methods.[8, 9]

Similar experiments (not shown) were performed for four and ten close-packed monolayers of $TiO_2$ nanocrystals deposited on conducting glass and fired at 450 °C for 2 h. The measured spectra are in good qualitative agreement with those measured for one monolayer although, as expected, the absorbance changes are correspondingly larger. Similar values for $V_{cb}$ at pH 2.0 and 12.0 were obtained.

The findings presented confirm that potentiostatic control of the Fermi potential ($V_f$) of a substrate consisting of

between one and ten close-packed monolayers of $TiO_2$ nanocrystals deposited on conducting glass, and by implication the $V_f$ of the nanocrystals constituting these monolayers, is possible.

### Preparation and characterisation of mixed monolayers of I and II at the air/water interface

Scheme 3 shows the structure of **I**.[14] Important features of this molecule include the following: Firstly, a phosphonic acid head group that is strongly chemisorbed at the surface of a $TiO_2$ nanocrystal,[15, 16] a property generally attributed to the Lewis basisity of the oxygen atoms of this group[17]; and secondly, an alkyl chain which endows this molecule with a sufficiently hydrophobic character to permit use of LB techniques to deposit an ordered monolayer on an appropriate substrate.[16]

Scheme 3 also shows the structure of **II.**[18] Important features of this molecule include the following: Firstly, a stable organic electron acceptor whose marked change in optical cross-section following reduction allows electron transfer to this molecule be monitored spectroscopically;[19] and secondly, symmetric alkyl chains, equal in length to those in **I**, which endow this molecule with a sufficiently hydrophobic character to permit use of LB techniques to deposit an ordered monolayer on an appropriate substrate and which minimise the possibility of phase separation.[17, 18, 20]

The surface pressure versus area isotherms for monolayers of **I** and **II** and mixtures of **I** and **II** are shown in Figure 3. These monolayers and mixed monolayers are denoted as follows: **A** (100% **I**), **B** (86% **I** and 14% **II**), **C** (75% **I** and 25% **II**), **D** (50% **I** and 50% **II**) and **E** (100% **II**).

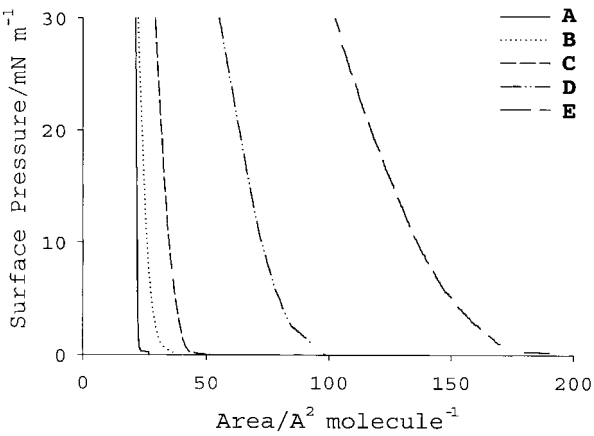


Figure 3. Surface pressure versus area isotherms for monolayers of **A** (100% **I**), **B** (86% **I** and 14% **II**), **C** (75% **I** and 25% **II**), **D** (50% **I** and 50% **II**) and **E** (100% **II**) conditioned by compression to 30 mN m$^{-1}$ on an aqueous subphase containing added KCl (0.1 mol dm$^{-3}$) at pH 5.5 and 25 °C.

The isotherm for **A** is close to ideal and displays the expected gas-to-liquid and liquid-to-solid transitions.[17] By extrapolating the linear (solid) region of the above isotherm to zero surface pressure a value of 22 Å$^2$ is obtained for the area occupied by a molecule in the hypothetical state of an uncompressed close-packed monolayer.[17] This value agrees well with that expected for **I** and implies that the alkyl chains of a compressed monolayer are close-packed in an all-*trans* configuration.[14, 17, 21] Recent studies of monolayers of long-chain aliphatic phosphonic acids at the air/water interface have shown this to be the case and have shown these monomers to have average tilt and twist angles of 1° and 43°, respectively, under similar conditions.[21]

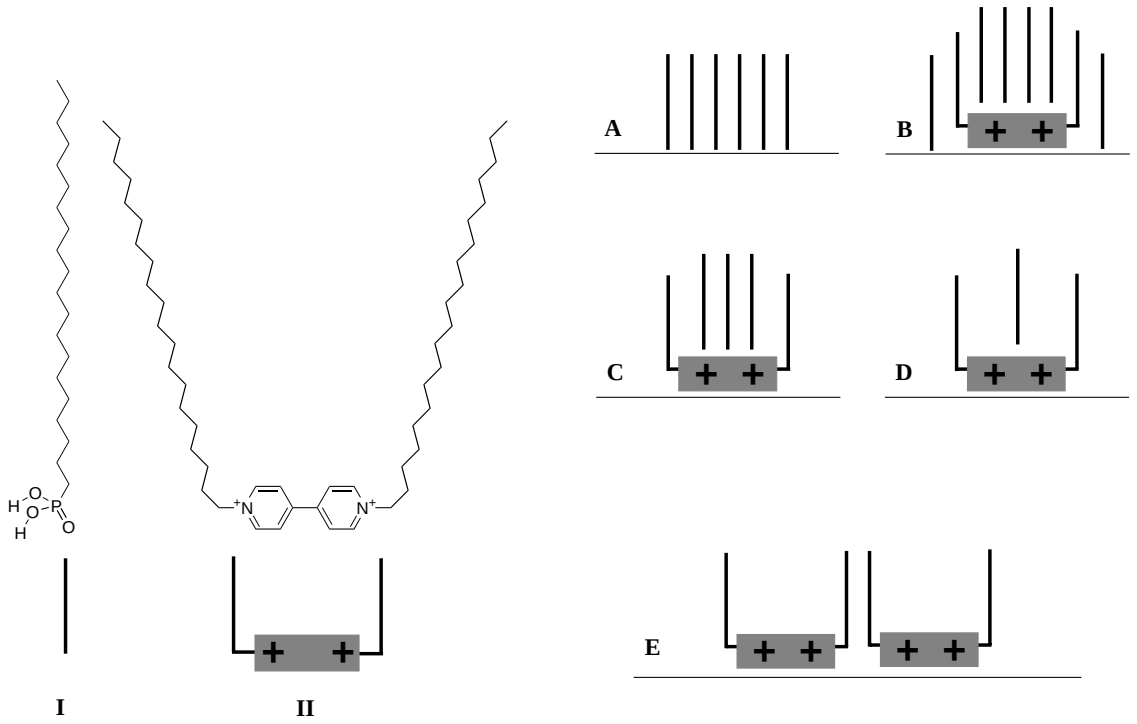


Scheme 3. The structure of **I** and **II** and schematic representations of the monolayers and mixed monolayers **A** (100% **I**), **B** (86% **I** and 14% **II**), **C** (75% **I** and 25% **II**), **D** (50% **I** and 50% **II**) and **E** (100% **II**).



0947-6539/01/0706-1312 $ 17.50+.50/0 *Chem. Eur. J.* **2001**, *7*, No. 6

The surface pressure versus area isotherm for **E** shows no distinct gas-to-liquid or liquid-to-solid transitions. By extrapolating the linear (solid) region of the above isotherm to zero surface pressure a value of 150 Å$^2$ is obtained for the area occupied by a molecule in the hypothetical state of an uncompressed close-packed monolayer.[17] This value agrees well with that expected for a close-packed monolayer of **II** in which each molecule is oriented (Scheme 3) with its bipyridine moiety parallel to air/water interface.[18] Implicit in the above, is that the alkyl chains of the constituent monomers are not close-packed and do not possess well defined average tilt or twist angles (see below).

The surface pressure versus area isotherms for **B**, **C** and **D** possess, to varying degrees, properties characteristic of the two limiting cases **A** and **E**. On the one hand, the isotherm measured for **B** is qualitatively similar to that measured for **A**. On the other hand, the isotherms measured for **C** and **D** are qualitatively similar to that measured for **E**.

More quantitatively, the average areas per molecule for a compressed monolayer of **A** and **E** are 22 Å$^2$ and 150 Å$^2$, respectively. On this basis, an average area per molecule of 40 Å$^2$ would have been predicted for a compressed monolayer of **B** (86 % **I** and 14 % **II**). The average area per molecule for **B** is found to be 27 Å$^2$. Similarly, an average area per molecule of 54 Å$^2$ would have been predicted for a compressed monolayer of **C** (75 % **I** and 25 % **II**). The average area per molecule for **C** is found to be 37 Å$^2$. Finally, an average area per molecule of 86 Å$^2$ would have been predicted for a compressed monolayer of **D** (50 % **I** and 50 % **II**). The average area per molecule is found to be 75 Å$^2$.

To account for these findings it is proposed, as previously reported and shown in Scheme 3,[18] that up to four **I** are incorporated in the cavity created by **II**. Consistent with this view, an average area per molecule of 27 Å$^2$ for **B** (**I**:**II** is 6:1) implies four of six **I** are accommodated inside the cavity created by **II**. Upon compressing a monolayer of **B**, as the cavity is 100 % occupied the isotherm observed is similar to that for **A** and suggests the alkyl chains are close-packed. Similarly, an average area per molecule of 37 Å$^2$ for **C** (**I**:**II** is 3:1) implies all **I** are accommodated inside the cavity created by **II**. Upon compressing a monolayer of **C** where the cavity is 75 % occupied, the isotherm observed is also similar to that for **A** and suggests the alkyl chains are essentially close-packed. Finally, an average area per molecule of 75 Å$^2$ for **D** (**I**:**II** is 1:1) implies all **I** are accommodated inside the cavity created by **II**. Upon compressing a monolayer of **D** where the cavity is only 25 % occupied, the isotherm observed is similar to that for **E** and suggests the alkyl chains are not close-packed. It is noted that the concentration of **II** is $5.2 \times 10^{13}$ cm$^{-2}$ in a compressed monolayer of **B**, while it is $6.7 \times 10^{13}$ cm$^{-2}$ in a compressed monolayer of **C**, **D** or **E**.

The findings presented confirm that the structures of the compressed monolayers and mixed monolayers **A** to **E** are as shown in Scheme 3.

### Deposition and characterisation of mixed monolayers of I and II on close-packed monolayers of $TiO_2$ nanocrystals

By way of notation, a monolayer of **A** deposited on a monolayer of close-packed $TiO_2$ nanocrystals is denoted $TiO_2$(1)-**A**. The same monolayer deposited on ten close-packed monolayers of $TiO_2$ nanocrystals is denoted $TiO_2$(10)-**A**. An analogous notation is used for a monolayer of **B** to **E** deposited on one to ten close-packed monolayer(s) of $TiO_2$ nanocrystals.

It is necessary to determine whether the structure of a monolayer of **A** to **E** at the air/water interface and deposited on one to ten close-packed monolayer(s) of $TiO_2$ nanocrystals is the same. Toward this end, a monolayer of **A** to **E** has been deposited on a close-packed monolayer of $TiO_2$ nanocrystals. The resulting organised assemblies, denoted $TiO_2$(1)-**A** to $TiO_2$(1)-**E**, have been characterised by polarised reflectance infrared reflection – absorption spectroscopy (IRRAS) and by potential dependent optical absorption spectroscopy.

The IRRAS of $TiO_2$(1)-**A** (Figure 4a) agrees well with that recently reported for a close-packed monolayer of a long-chain aliphatic phosphonic acid deposited on a monolayer of

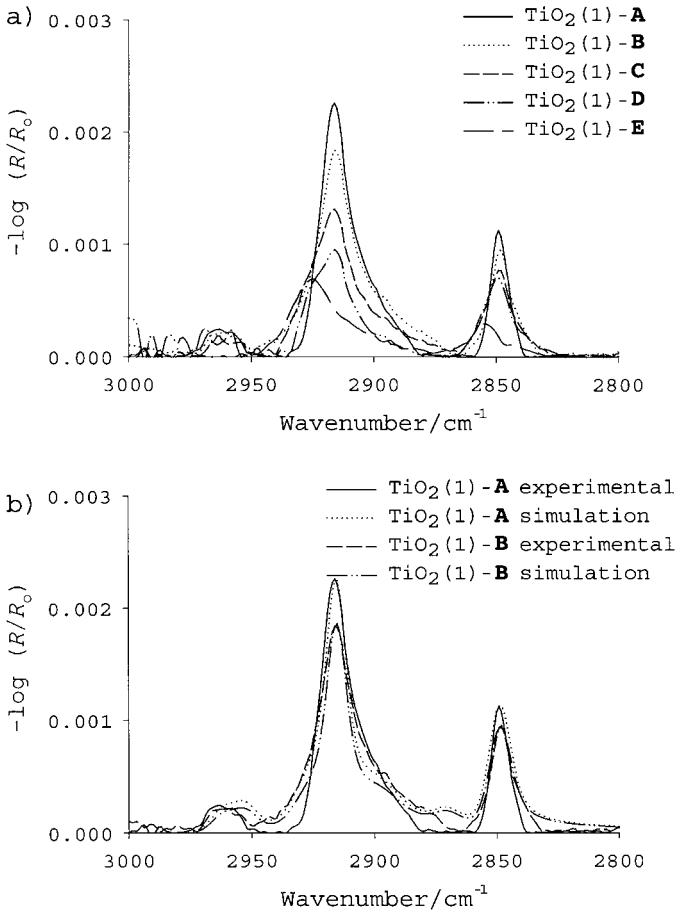


Figure 4. a) IRRAS of $TiO_2$(1)-**A**, $TiO_2$(1)-**B**, $TiO_2$(1)-**C**, $TiO_2$(1)-**D** and $TiO_2$(1)-**E**. Spectra were measured using p-polarised light at an angle of incidence of 73° and against a background spectrum recorded for $TiO_2$(1). b) Comparison of the IRRAS measured and simulated for $TiO_2$(1)-**A** and $TiO_2$(1)-**B**.

$TiO_2$ nanocrystals.[14, 21] The bands observed at 2917 cm$^{-1}$ (0.0023 au) and 2850 cm$^{-1}$ (0.0012 au) are assigned to the asymmetric and symmetric -$CH_2$- stretches of **I**,respectively. The magnitude of these absorptions confirm that a monolayer is present.[14, 21] The frequency of these bands confirm that the

deposited monolayer is constituted from molecules close-packed in an all-*trans* configuration.[14, 21] More quantitatively, the measured IRRAS has been simulated by using the method of Allara and co-workers (see Figure 4b and Table 1).[22] The values determined for the average tilt and twist angles of the constituent monomers of $TiO_2$(1)-**A** are 17° and 48°, respectively.

Table 1. Characterisation of mixed monolayers of **I** and **II** deposited on a monolayer of close-packed $TiO_2$ nanocrystals.[a]

| Property | $TiO_2$(1)-**A** | $TiO_2$(1)-**B** | $TiO_2$(1)-**C** | $TiO_2$(1)-**D** | $TiO_2$(1)-**E** |
|---|---|---|---|---|---|
| extrapolated surface area [Å$^2$ per molecule] | 22 | 27 | 37 | 75 | 150 |
| asymmetric $CH_2$ stretch [cm$^{-1}$] | 2917 | 2916 | 2917 | 2917 | 2929 |
| symmetric $CH_2$ stretch [cm$^{-1}$] | 2850 | 2848 | 2850 | 2849 | 2855 |
| average tilt angle [°] determined | 17 | 13 | 17 | 29 | noted |
| average twist angle [°] determined | 13 | 48 | 47 | 45 | noted |

[a] Monolayers were conditioned on an aqueous subphase at pH 5.5 and 25 °C and deposited at 30 mN m$^{-1}$ on a substrate consisting of a close-packed monolayer of $TiO_2$ nanocrystals deposited on F-doped tin oxide glass.

The IRRAS of $TiO_2$(1)-**B** (Figure 4a) agrees well with that measured for $TiO_2$(1)-**A**. The bands observed at 2916 cm$^{-1}$ (0.0018 au) and 2848 cm$^{-1}$ (0.0010 au) are assigned to asymmetric and symmetric -$CH_2$- stretches, respectively. The frequency and magnitude of these absorptions confirm the presence of a monolayer close-packed molecule in an all-*trans* configuration.[14, 21] The above spectrum has also been simulated using the method of Allara and co-workers (see Figure 4b and Table 1).[22] The values determined for the average tilt and twist angles of the constituent monomers of $TiO_2$(1)-**B** are 13° and 48°, respectively.

The IRRAS of $TiO_2$(1)-**C** to $TiO_2$(1)-**E** (Figure 4a) differ qualitatively from those measured for $TiO_2$(1)-**A** and $TiO_2$(1)-**B**. Specifically, the bands assigned to the asymmetric and symmetric -$CH_2$- stretches shift to higher frequencies, decrease in intensity and broaden significantly on going from $TiO_2$(1)-**B** to $TiO_2$(1)-**E**. The bands broaden and shift to higher frequencies due to the increasingly liquid-like state of the deposited monolayer. The reduced intensity is due to a decrease in the number of alkyl chains per unit area. Both are a consequence of the cavity within **II** progressively emptying on going from $TiO_2$(1)-**B** to $TiO_2$(1)-**E** as shown in Scheme 3. These spectra have also been simulated by using the method of Allara and co-workers (see Table 1).[22, 23] The values determined for the average tilt angles of $TiO_2$(1)-**C** and $TiO_2$(1)-**D** are 17° and 29° respectively. The values determined for the average twist angles of $TiO_2$(1)-**C** and $TiO_2$(1)-**D** are 47° and 45°, respectively. The corresponding values for $TiO_2$(1)-**E** could not be determined as the measured spectrum is that of an entirely liquid-like monolayer.

The potential-dependent optical absorption spectra of $TiO_2$(1)-**A** to $TiO_2$(1)-**E** have been measured at pH 2.0 and an applied potential of −0.80 V. As expected, the spectrum measured for $TiO_2$(1)-**A** (not shown) agrees well with that measured for $TiO_2$(1) (Figure 2a) as in both cases the measured spectrum is assigned to electrons occupying the available states of the conduction band. The spectra measured for $TiO_2$(1)-**B** and $TiO_2$(1)-**E** are shown in Figure 5 and are assigned to electrons occupying the available states of the conduction band and to the radical cation of the viologen **II**.[9, 19] It is noted, that the radical cation component of the spectrum measured for $TiO_2$(1)-**B** is less intense than that the same component measured for $TiO_2$(1)-**E**. It is noted also, as expected, that the intensity of the radical cation component of the spectra measured for $TiO_2$(1)-**C** (not shown) to $TiO_2$(1)-**E** is constant.

More quantitatively, as the first reduction potential of the bipyridine moiety of **II** is −0.5 V (SCE)[18, 24] and as $V_{cb}$ for the nanocrystal substrate is −0.6 V,[9] it is assumed all **II** are reduced at an applied potential of −0.80 V. On this basis, and taking a value of $1.37 \times 10^4$ mol$^{-1}$ dm$^3$ cm$^{-1}$ for the extinction coefficient of the radical cation of **II** in water at 550 nm,[19] we predict absorbances of 0.0013 au and 0.0015 au for $TiO_2$(1)-**B** and $TiO_2$(1)-**E**, respectively. These values agree well with those measured. The lower absorbance by the radical cation of **II** in $TiO_2$(1)-**B**, compared to that for $TiO_2$(1)-

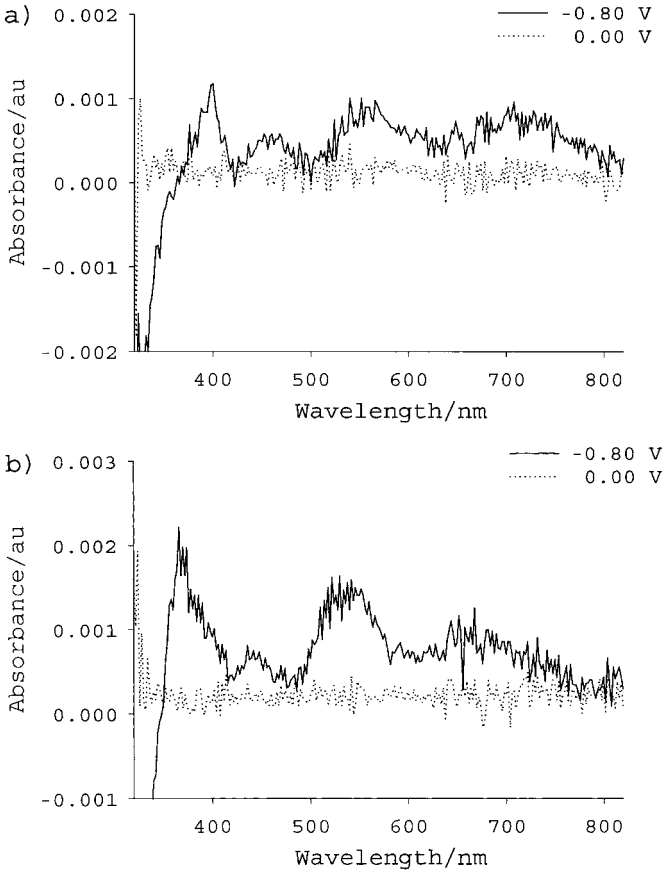


Figure 5. a) Potential-dependent optical absorption spectra of $TiO_2$(1)-**B**. Spectra were measured at pH 2.0 and the indicated applied potentials versus SCE against a background spectrum measured at 0.00 V. b) As in a) for $TiO_2$(1)-**E**.



0947-6539/01/0706-1314 $ 17.50+.50/0 *Chem. Eur. J.* **2001**, *7*, No. 6

**E**, is due to the lower surface concentration of adsorbed **II** in $TiO_2(1)$-**B**.

The findings presented confirm that the structure of a monolayer **A** to **E** at the air/water interface (Scheme 3) and deposited on a close-packed monolayer of $TiO_2$ nanocrystals in $TiO_2(1)$-**A** to $TiO_2(1)$-**E** (Scheme 4) are similar. These findings also confirm that the alkyl chains of **I** and **II** are close packed in an all-*trans* configuration in **A** to **C** but not **D** and **E**. As discussed in detail elsewhere, the principal difference between these monolayers at the air/water interface and deposited on a close-packed monolayer of $TiO_2$ nanocrystals is the average tilt angles of the monomers.[21] In accordance with these findings, the organised assemblies $TiO_2(1)$-**B** and $TiO_2(1)$-**E** are represented as shown in Scheme 4.

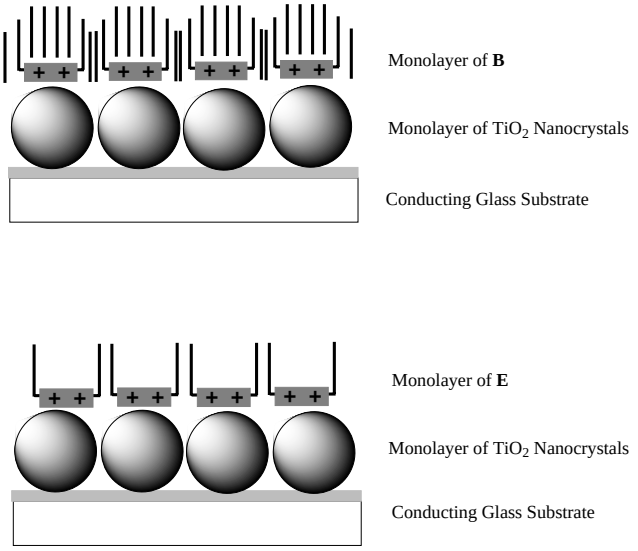


Scheme 4. Schematic representations of the organised assemblies $TiO_2(1)$-**B** (top) and $TiO_2(1)$-**E** (bottom).

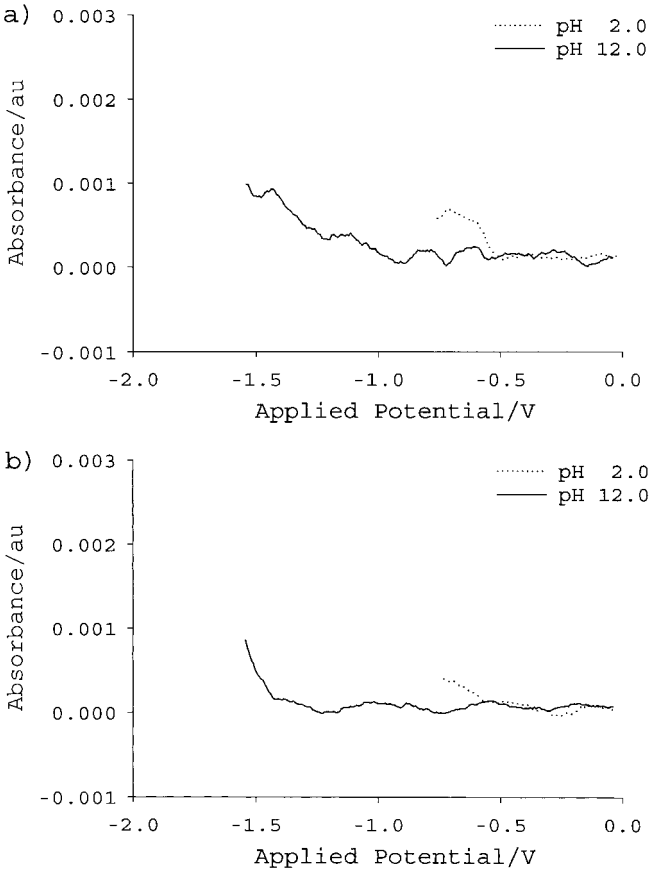


Figure 6. a) Absorbance increase at 550 nm of $TiO_2(1)$-**E**. Absorbance changes were measured at the indicated pH and applied potentials versus SCE against a background measured at 0.00 V. b) As in a) for $TiO_2(10)$-**E**.

### Elimination of cross-talk in an organised heterosupramolecular assembly

The organised heterosupramolecular assembly $TiO_2(1)$-**B** consists of a monolayer of close-packed $TiO_2$ nanocrystals on which has been deposited a close-packed mixed monolayer of **B** (see Scheme 4). Under these conditions, there are an average of two **II** adsorbed at each nanocrystal, each with their viologen moiety oriented parallel to the nanocrystal surface and isolated from each other by co-adsorbed **I**. For this reason, it is expected that electron transfer between adjacent viologens in the organised heterosupramolecular assembly $TiO_2(1)$-**B** will be inhibited. To test this expectation, the potential dependent optical absorption spectroscopy of $TiO_2(1)$-**B** to $TiO_2(10)$-**B** and $TiO_2(1)$-**E** to $TiO_2(10)$-**E** has been studied in detail.

Figure 6a shows the results of experiments at pH 2.0 and 12.0 in which absorption by $TiO_2(1)$-**E** at 550 nm was monitored as a function of applied potential. The absorbance increase at 550 nm is assigned to electrons occupying the available states of the conduction band and to the formation of the radical cation of **II**.[9, 19] At pH 2.0, it is found that electrons occupy the available states of the conduction band and **II** is reduced at applied potentials more negative than $-0.6$ V. This finding is consistent with the first reduction potential of **II** ($-0.5$ V) and $V_{cb}$ ($-0.6$ V) having similar values. At pH 12.0, it is found that **II** is reduced at applied potentials more negative than the first reduction potential of **II** but more positive than $V_{cb}$ ($-1.2$ V). Electrons occupy the available states of the conduction band at applied potentials more negative than $V_{cb}$. This finding is consistent with the first reduction potential of **II** ($-0.5$ V) and $V_{cb}$ ($-1.2$ V) having significantly different values.

Similar experiments were performed for $TiO_2(4)$-**E** (not shown) and $TiO_2(10)$-**E** (Figure 6b). At pH 2.0, **II** is reduced and electrons occupy the available states of the conduction band at applied potentials more negative than $-0.6$ V. At pH 12.0, **II** is reduced at applied potentials close to or more negative than $V_{cb}$. Specifically, **II** is reduced at applied potentials more negative than $-0.9$ V and $-1.2$ V for $TiO_2(4)$-**E** and $TiO_2(10)$-**E**, respectively. Electrons occupy the available states of the conduction band at applied potentials more negative than $V_{cb}$.

Qualitatively and quantitatively different behaviour is observed for $TiO_2(1)$-**B** to $TiO_2(10)$-**B**. Specifically, **II** is reduced at applied potentials more negative than $V_{cb}$ at both pH 2.0 and pH 12.0 for $TiO_2(1)$-**B**, $TiO_2(4)$-**B** (not shown) and $TiO_2(10)$-**B** (Figure 7).

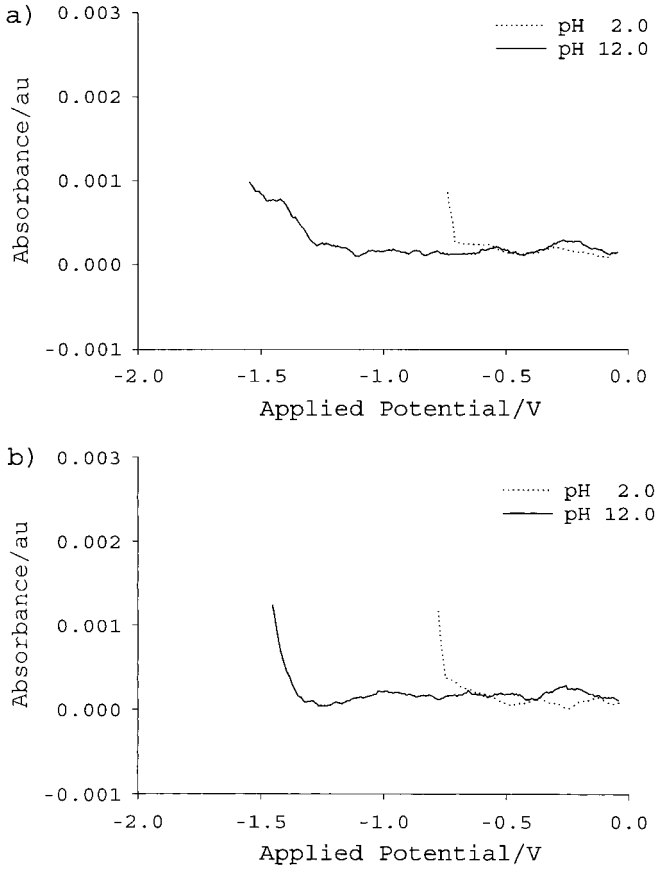


Figure 7. a) Absorbance increase at 550 nm of $TiO_2(1)$-**B**. Absorbance changes were measured at the indicated pH and applied potentials versus SCE against a background measured at 0.00 V. b) As in a) for $TiO_2(10)$-**B**.

These findings are consistent with **II** in $TiO_2(1)$-**E** and $TiO_2(4)$-**E** being reduced by electron transfer directly from the conducting glass substrate and/or by trap mediated (bulk or surface) electron transfer from a nanocrystal. That is, occupation of the available conduction band states by electrons is not a pre-requisite for reduction of **II**. These findings are also consistent with the viologen **II** in $TiO_2(10)$-**E** being reduced by conduction band state mediated electron transfer from a nanocrystal. That is, occupation of the available conduction band states by electrons is a pre-requisite for reduction of **II**.

In apparent contradiction is the finding that for $TiO_2(1)$-**B** to $TiO_2(10)$-**B** occupation of the available conduction band states by electrons is a pre-requisite for reduction of **II**. Clearly, direct electron transfer from the conducting glass substrate and/or trap state mediated electron transfer from a $TiO_2$ nanocrystal to **II** is less important in $TiO_2(1)$-**B** and $TiO_2(4)$-**B** than in $TiO_2(1)$-**E** and $TiO_2(4)$-**E**. This apparent contradiction is resolved by proposing that direct and/or trap state mediated electron transfer is important in $TiO_2(1)$-**E** and $TiO_2(4)$-**E** because it is accompanied by electron transfer from one viologen to another, that is cross-talk. It is likely that the existence of a number of hot-spots, where direct and/or trap state mediated electron transfer is pronounced, leads to reduction of a significant fraction of **II**. In $TiO_2(1)$-**B** and $TiO_2(4)$-**B** the presence of co-adsorbed **I** prevents electron transfer from one viologen to another and cross-talk is inhibited. Under these conditions conduction band state mediated electron transfer dominates.

The findings presented confirm that electron transfer between adjacent viologens in $TiO_2(1)$-**B** to $TiO_2(10)$-**B** is inhibited. Or, in other words, that each heterosupermolecule in the heterosupramolecular assemblies $TiO_2(1)$-**B** to $TiO_2(10)$-**B** acts independently.

### Function modulation in an organised heterosupramolecular assembly

Detailed characterisation of the heterosupramolecular assembly $TiO_2(1)$-**B** has established that it is organised as shown in Scheme 4. As a consequence, each heterosupermolecule within the assembly is individually addressable. Furthermore, each heterosupermolecule is isolated within the assembly and cross-talk is inhibited. It remains, therefore, to demonstrate that the heterosupramolecular function of the above assembly is light induced vectorial electron transfer and that this function may be modulated potentiostatically.

Toward these ends, the $TiO_2$ nanocrystal components in $TiO_2(10)$-**E** and $TiO_2(10)$-**B** were excited at 355 nm and electron transfer to **II** monitored in real-time at 630 nm under open circuit conditions and at a positive applied potential (+0.60 V). These experiments could not be performed for $TiO_2(1)$-**E** and $TiO_2(1)$-**B** or $TiO_2(4)$-**E** and $TiO_2(4)$-**B** as the optical cross-section at 355 nm was not sufficient to generate a measurable concentration of reduced **II**.

Figure 8a shows absorption transients measured following bandgap excitation of $TiO_2(10)$-**E** and $TiO_2(10)$-**A** under open circuit conditions. The transient for $TiO_2(10)$-**E** is assigned to trapped electrons and to the radical cation of **II**, while the transient for $TiO_2(10)$-**A** is assigned to trapped electrons.[5] At a positive applied potential (+0.60 V) the transients for $TiO_2(10)$-**E** and $TiO_2(10)$-**A** are similarly assigned (Figure 8b). The difference of the transients measured for $TiO_2(10)$-**E** and $TiO_2(10)$-**A** under open circuit conditions and at a positive applied potential (+0.60 V) are plotted in Figure 8c.

The difference transients in Figure 8c show that under open circuit conditions the radical cation of **II** is formed over a period of about 0.5 μs and is long-lived. At a positive applied potential no radical cation is formed in the first 0.5 μs following bandgap excitation although, radical cation formation is observed on a slower time scale. The concentration of radical cation reaches a maximum after 2 μs and subsequently decays at the same rate as the transient assigned to trapped electrons.

Figure 9a shows absorption transients measured following bandgap excitation of $TiO_2(10)$-**B** and $TiO_2(10)$-**A** under open circuit conditions. The transient for $TiO_2(10)$-**B** is assigned to trapped electrons and to the radical cation of **II**, while the transient for $TiO_2(10)$-**A** is assigned to trapped electrons.[5] At a positive applied potential (+0.60 V) the transients for $TiO_2(10)$-**B** and $TiO_2(10)$-**A** are similarly assigned (Figure 9b). The difference of the transients measured for $TiO_2(10)$-**B** and $TiO_2(10)$-**A** under open circuit conditions and at a positive applied potential (+0.60 V) are plotted in Figure 9c.



0947-6539/01/0706-1316 $ 17.50+.50/0 *Chem. Eur. J.* **2001**, *7*, No. 6

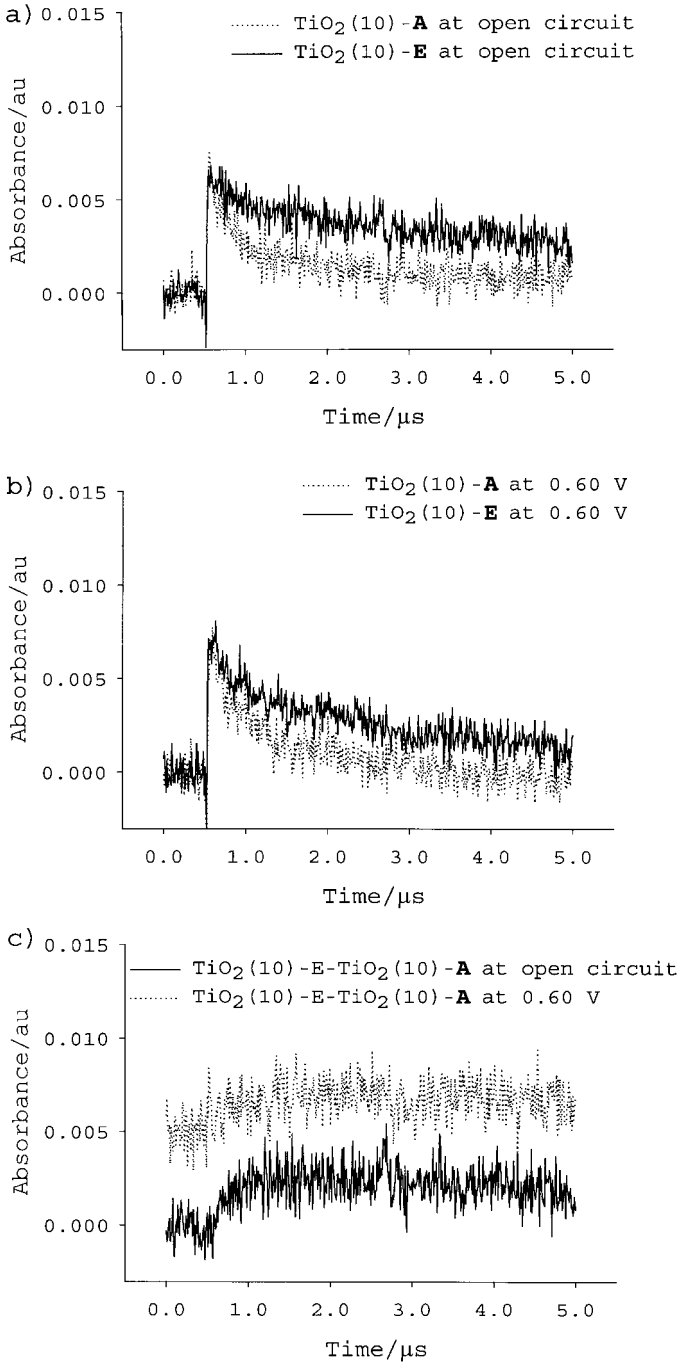


Figure 8. a) Transient absorbance at 630 nm measured following pulsed excitation at 355 nm (15 mJ per pulse, single shot) of $TiO_2$(10)-**E** and $TiO_2$(10)-**A** under open circuit conditions. b) As in a) for $TiO_2$(10)-**E** and $TiO_2$(10)-**A** at an applied potential of +0.60 V versus SCE. c) Difference of transients measured in a) and b).

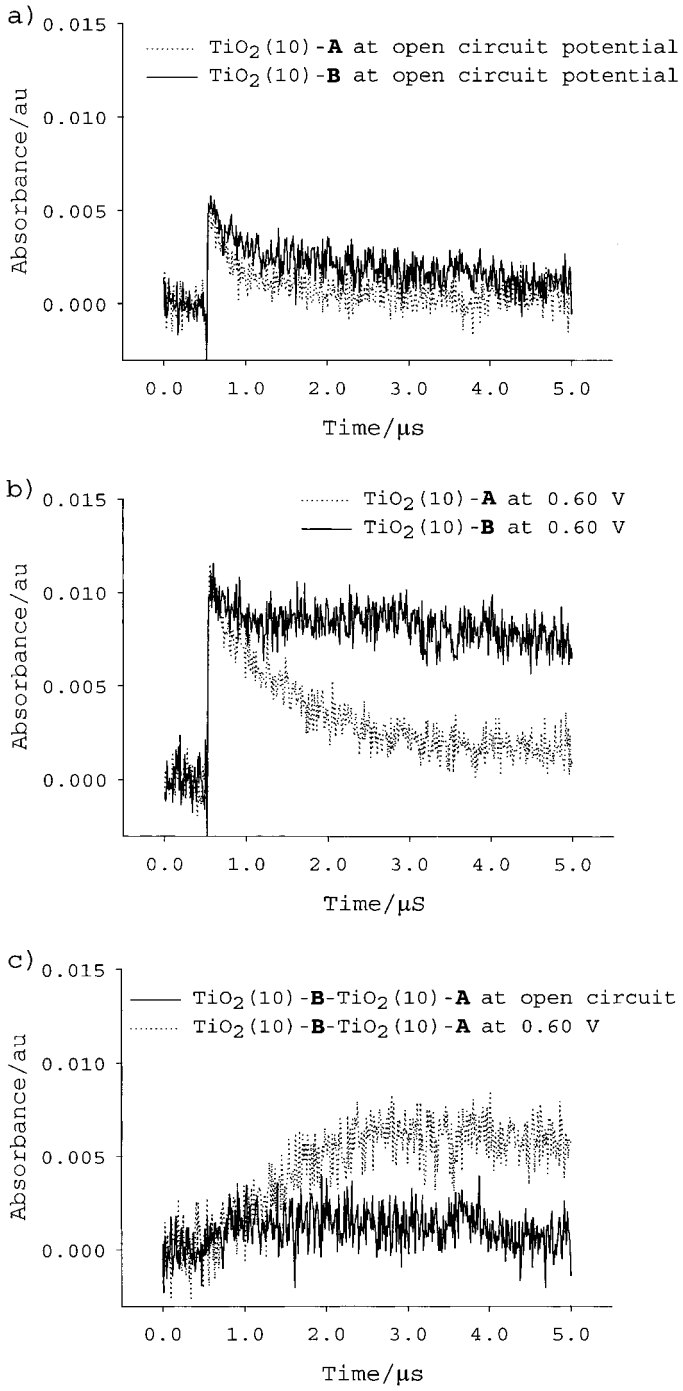


Figure 9. a) Transient absorbance at 630 nm measured following pulsed excitation at 355 nm (15 mJ per pulse, single shot) of $TiO_2$(10)-**B** and $TiO_2$(10)-**A** under open circuit conditions. b) As in a) for $TiO_2$(10)-**B** and $TiO_2$(10)-**A** at an applied potential of +0.60 V versus SCE. c) Difference of transients measured in a) and b).

The difference transients in Figure 9c show that under open circuit conditions the radical cation of **II** is formed over a period of about 0.5 μs and is long-lived. At a positive applied potential no radical cation is formed in the first 0.5 μs following bandgap excitation although, radical cation formation is observed on a slower time scale. The concentration of radical cation reaches a maximum after 2.5 μs and subsequently decays.

Clearly, the above data analysis is predicated on an assumption that the concentration of trapped electrons and their decay kinetics are not affected by the presence of a molecular monolayer adsorbed at the surface of the nanostructured film. Bearing in mind, however, that there are ten monolayers of nanocrystals and that only one of these layers is in contact with the deposited molecular monolayer, this appears reasonable.

Function modulation is assumed to be effective for the following reasons: At the open circuit potential, $V_f$ is close to $V_{cb}$ permitting reduction of **II** (see Scheme 5). Specifically, the

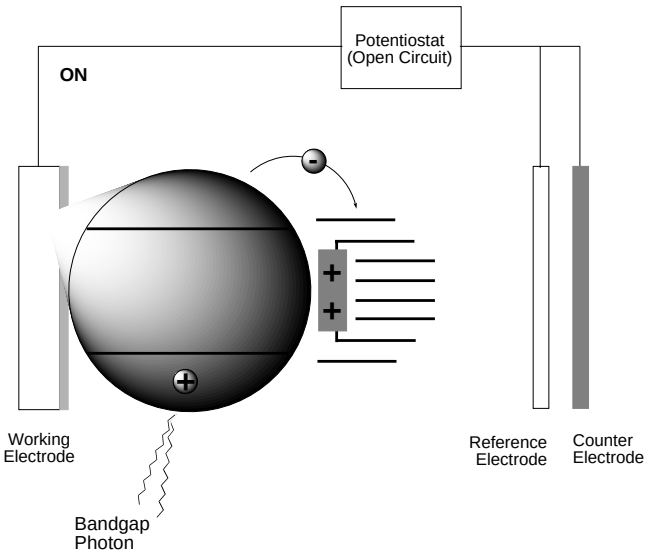


Scheme 5. Schematic representation of the process that occurs when an open circuit potential is applied; $V_f$ is close to $V_{cb}$ and reduction of **II** is permitted.

generation of electron-hole pairs by bandgap excitation results in electron transfer from the conduction band of a $TiO_2$ nanocrystal to the viologen moiety in **II**. At the positive applied potential, $V_f$ is positive of $V_{cb}$ preventing reduction of the viologen moiety of **II** (see Scheme 6). Specifically, the

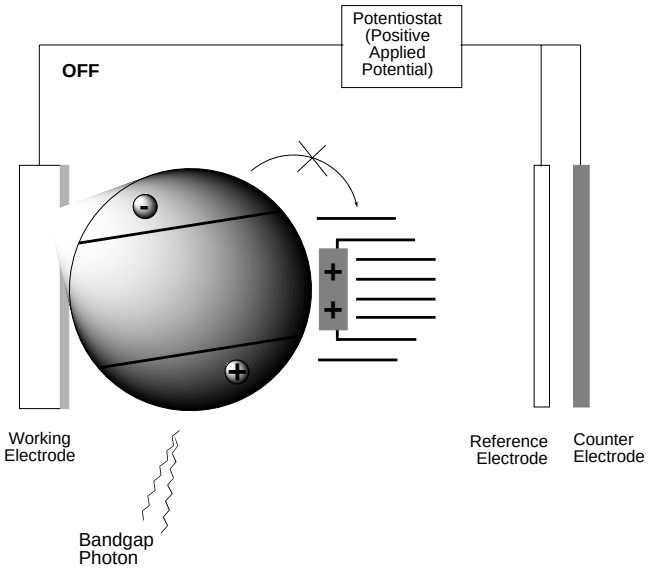


Scheme 6. Schematic representation of the process that occurs when a positive applied potential is used; $V_f$ is positive of $V_{cb}$ and reduction of the viologen moiety of **II** is prevented.

generation of electron-hole pairs by bandgap excitation results in electron transfer to the conducting glass substrate.

The findings confirm that, depending on the potential applied to the heterocomponents of the heterosupramolecular assembly, the function of the constituent heterosupermolecules (light-induced electrons transfer) may be modulated between an ON state under open circuit conditions and OFF state at +0.60 V (see Scheme 5 and Scheme 6, respectively). Further, that the modulation state of the constituent heterosupermolecules may be inferred if the potential applied to heterocomponents constituting the heterosupramolecular assembly is known.

Clearly, there is also a mechanism by which the radial cation of the viologen moiety in **II** is formed and subsequently decays in both $TiO_2$(10)-**E** and $TiO_2$(10)-**B**. In this context it is noted that an important difference between $TiO_2$(10)-**E** and $TiO_2$(10)-**B** is that in the former the viologen moieties in **II** are not insulated from each other by co-adsorbed **I** and electron transfer between these moieties is uninhibited, while in the latter the viologen moieties in **II** are isolated from each other by co-adsorbed **I** and electron transfer between these moieties is inhibited.

At the open circuit potential all the viologen moieties in $TiO_2$(10)-**E** and $TiO_2$(10)-**B** are reduced following bandgap excitation by electron transfer from the nanocrystal at which a viologen is adsorbed. This process is largely complete after 0.5 $\mu$s and the radical cations of **II** which are formed are long-lived as the trap states, which mediate their oxidation, are filled with electrons.

At a positive applied potential there is no direct electron transfer, following bandgap excitation, from a nanocrystal to an adsorbed viologen in either $TiO_2$(10)-**E** or $TiO_2$(10)-**B** (see Scheme 6). There is, however, electron transfer from filled trap states to the viologens in the molecular monolayer adsorbed at the surface of the outermost of the ten monolayers of $TiO_2$ nanocrystals. In the case of $TiO_2$(10)-**E** the rates at which these electrons migrate into the adsorbed monolayer of **II** is relatively fast as electron transfer between these viologens is uninhibited. The rate at which these electrons migrate out of the adsorbed monolayer is also relatively fast as this is the rate at which the trap states are being emptied at a positive applied potential. As a consequence, the steady state concentration of reduced **II** is relatively low. In the case of $TiO_2$(10)-**B** the rates at which these electrons migrate into the adsorbed monolayer of **II** is relatively slow as electron transfer between **II** is inhibited. The rate at which these electrons migrate out of the adsorbed monolayer is also relatively slow, that is slower than the rate at which the trap states are being emptied at a positive applied potential. As a consequence, the steady-state concentration of reduced **II** is relatively high.

## Conclusion

Having undertaken a detailed characterisation of the organised heterosupramolecular assemblies $TiO_2$(1)-**E** to $TiO_2$(10)-**E**, it is possible to state the following: Firstly, each viologen is adsorbed in monomeric form with its bipyridine moiety flat on the nanocrystal substrate; secondly, there are less than three viologens adsorbed at each nanocrystal; thirdly, electron transfer between neighbouring viologens, that is cross-talk, is uninhibited; fourthly, at a sufficiently negative applied potential the viologens in $TiO_2$(1)-**E** and $TiO_2$(4)-**E** are reduced either by direct electron transfer from the conducting glass substrate or by trap state mediated electron transfer



0947-6539/01/0706-1318 $ 17.50+.50/0 *Chem. Eur. J.* **2001**, *7*, No. 6

from a nanocrystal followed by electron transfer to nearest neighbour viologens; and finally, at sufficiently negative applied potentials the viologens in $TiO_2$(10)-**E** are reduced by conduction band state mediated electron transfer from a nanocrystal followed by electron transfer to nearest neighbour viologens.

Having undertaken a detailed characterisation of the organised heterosupramolecular assemblies $TiO_2$(1)-**B** to $TiO_2$(10)-**B** it is possible to state the following: Firstly, each viologen is adsorbed in monomeric form with its bipyridine moiety flat on the nanocrystal substrate; secondly, there are less than two viologens adsorbed at each nanocrystal; and finally, because these viologens are partially isolated by a co-adsorbed long-chain aliphatic acid, electron transfer between neighbouring viologens is inhibited.

Based on the above findings it was asserted that the organised heterosupramolecular assembly $TiO_2$(1)-**B** is accurately represented in Scheme 4; that each heterosupermolecule is individually addressable; that each heterosupermolecule will act independently within the assembly; and that function modulation will be effective and accounted for by a well-understood mechanism.

Concerning the first of these properties, since the heterosupramolecular assembly is organised each of the constituent heterosupermolecules in $TiO_2$(1)-**B** is in principle addressable. To date, however, it has not proved possible for the following technical reasons to address a single heterosupermolecule: Firstly, there are two viologens adsorbed at each nanocrystal; and secondly, the technology necessary to selectively irradiate a nanocrystal and to monitor to the absorption change accompanying the subsequent electron transfer to the viologen is not routinely available. Toward this end, the ratio of **I** to **II** has been increased to 12:1, thereby reducing the number of viologens per nanocrystal to one. Furthermore, work has commenced on the development of a modified near-field scanning optical microscope that will permit individual heterosupermolecules to be addressed.

Concerning the second of these properties, it has clearly been demonstrated that even for ratios of **I**:**II** of 6:1 in $TiO_2$(1)-**B** electron transfer between nearest neighbour viologens on the same or different nanocrystals is inhibited. Furthermore, because each nanocrystal is separated by about 3 Å, electron transfer between nanocrystals is not expected to be an important process. In short, each of the heterosupermolecules in the assembly acts independently.

Concerning the third point, function modulation can be assumed to be effective in $TiO_2$(10)-**B**. On the one hand, for $TiO_2$(10)-**B** under open circuit conditions each photogenerated electron-hole pair results in formation of a radical cation. On the other hand, at a positive applied potential no electron transfer is observed. In short, the heterosupramolecular function associated with each heterosupermolecule in the assembly, light-induced vectorial electron transfer, is efficiently modulated between an ON state (at the open circuit potential) and an OFF state (at a positive applied potential). Further, the modulation state (ON or OFF) of each of the constituent heterosupermolecules of the assembly may be inferred if the potential applied to the intrinsic substrate or individual nanocrystals is known.

## Experimental Section

**Synthesis of condensed-phase component**

$TiO_2$ nanocrystals were prepared as described by Kotov et al.[6] Briefly, a solution of titanium tetraisopropoxide in 2-propanol (1.125 mL, 1:9 by volume) was added to chloroform (60 mL) and 2-propanol (40 mL) containing excess water (150 μL present in added catalyst). The above addition was carried out in the presence of cetyltrimethylammonium bromide stabiliser (0.015 g) and tetramethylammonium hydroxide catalyst (0.2 g, 75 % by wt. water). The resulting sol was refluxed at 90 °C for 90 min. Characterisation was by optical absorption spectroscopy, using a Hewlett-Packard 8452A diode array spectrophotometer, and by transmission electron microscopy, using a JEOL 2000 TEMSCAN. The measured onset for absorption and average nanocrystal diameter, $370 \pm 10$ nm and $23 \pm 2$ Å, respectively, are in good agreement with previously reported values.[6, 7]

**Synthesis of molecular components**

The molecular components eicosyl phosphonic acid (**I**) and 1,1′-dieicosyl-4,4′-bipyridinium dichloride (**II**) were used in the course of the studies reported.

**Preparation of I**

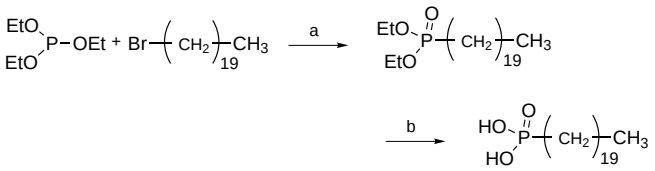


**I**

Scheme 7. Reagents and conditions for the preparation of **I**: a) neat reflux; b) 50 % HCl, reflux.

Component **I** was prepared as shown in Scheme 7. Elemental analysis (%) calcd for $C_{20}H_{43}O_3P$: C 66.26, H 11.96, P 8.54; found: C 66.00, H 12.05, P, 8.06; $^1$HNMR ([D]chloroform): $\delta = 0.88$ (t, $J = 7.6$ Hz, 3H), $\delta$ 1.2–1.3 (unresolved m, 34H), 1.84 (m, 2H), 3.43 (m, 2H).

**Preparation of II**

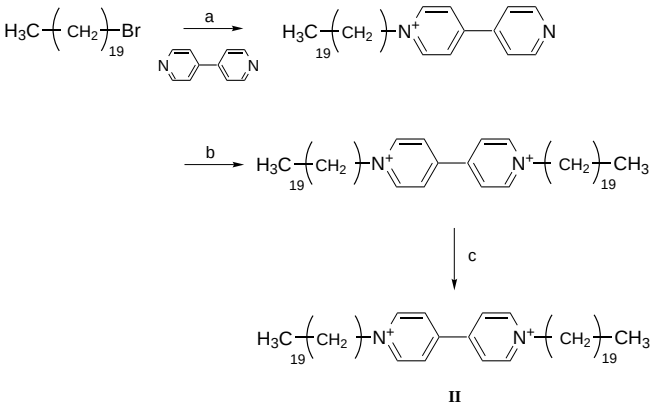


**II**

Scheme 8. Reagents and conditions for the preparation of **II**: a) acetone reflux; b) bromoeicosane, acetonitrile, reflux; c) reflux in HCl (10 % v/v).

Component **II** was prepared as shown in Scheme 8. Elemental analysis (%) calcd for $C_{50}H_{90}N_2Cl_2 \cdot 4H_2O$: C 69.76, H 11.39, N 3.25, Cl 8.14; found: C 69.61, H 11.66, N 3.32, Cl 8.35; $^1$HNMR ([D]trifluoroacetic acid): $\delta = 0.84$ (t, $J = 7.6$ Hz, 6H), 1.27–1.44 (m, 68H), 2.04–2.14 (m, 4H), 4.71–4.76 (t, $J = 7.33$, 4H), 8.61–8.63 (dd, $J = 5.86$, 4H, unresolved), 9.03–9.05 (dd, $J = 5.86$, 4H unresolved).

**Preparation of organised heterosupramolecular assemblies**

The required number of monolayers of close-packed $TiO_2$ nanocrystals were deposited on F-doped tin oxide glass (0.5 μm, 8 Ω square$^{-1}$, Nippon

Sheet Glass Company) using a JL Automation Langmuir Minitrough.[8] Briefly, hexane (20 mL) was added to the $TiO_2$ sol (100 mL) whose preparation has been described above. The resulting stock solution (300 μL) was spread, using a precision syringe, on the surface of the aqueous subphase at pH 5.5 and 25 °C. Having allowed 1 h for solvent evaporation, the resulting monolayer was conditioned by successive compression-expansion cycles to 25 mN m$^{-1}$. Maintaining the above monolayer at 25 mN m$^{-1}$ for 30 min resulted in an additional 25 % decrease in surface area. Subsequent compression-expansion cycles to 30 mN m$^{-1}$ were highly reversible and resulted in a final area per particle of about 550 Å$^2$ at 30 mN m$^{-1}$. Two pieces of conducting glass; mounted back-to-back and previously dipped were raised at a rate of 20 mm min$^{-1}$ through a conditioned monolayer of $TiO_2$ nanocrystals compressed to 30 mN m$^{-1}$. Deposition occurs on both sides of the glass and is observed only on the up-stroke. Prior to deposition of a second monolayer, the conducting glass substrates were maintained in the raised position and allowed to dry for about 15 min. They were then dipped and raised again to deposit the additional monolayers. To remove the organic material, the deposited monolayer or monolayers were fired at 450 °C for 2 h.

A monolayer of the required molecular components was deposited, also using a JL Automation Langmuir Minitrough, on the required number of previously fired monolayers of $TiO_2$ nanocrystals on conducting glass. Briefly, stock solutions of **I** in chloroform and **II** in chloroform/methanol (20 % by vol.) were prepared. Stock solutions containing **I** and **II** in the following proportions were then prepared: **A** (100 % **I**), **B** (86 % **I** and 14 % **II**), **C** (75 % **I** and 25 % **II**), **D** (50 % **I** and 50 % **II**) and **E** (100 % **II**). The required volume (between 150 μL and 450 μL) of stock solution ($3.5 \times 10^{-4}$ mol dm$^{-3}$) was spread, using a precision syringe held, on the surface of the aqueous subphase containing added KCl (0.1 mol dm$^{-3}$) at pH 5.5 and 25 °C. Having allowed 1 h for solvent evaporation, the resulting monolayers was conditioned by compression at a barrier rate of 30 mm min$^{-1}$ to a final surface pressure of 30 mN m$^{-1}$. Finally, two substrates mounted back-to-back and previously dipped, were raised at a rate of 20 mm min$^{-1}$ through a conditioned monolayer compressed to 30 mN m$^{-1}$. Deposition, which occurs on both substrates, is observed only on the up-stroke.

**Infrared reflection absorption spectroscopy**

Infrared reflection absorption spectroscopy was used to characterise the monolayers prepared from the stock solutions **A** to **E** above following their deposition on a close-packed monolayer of $TiO_2$ nanocrystals supported on conducting glass. Specifically, a variable-angle reflection accessory (Graseby-Specac) was placed in the sample compartment of a FT-IR spectrometer (Mattson Infinity) equipped with a MCT detector (liquid nitrogen cooled). The sample compartment was purged with nitrogen prior to and during data acquisition. Spectra were recorded at 2 cm$^{-1}$ resolution (one zero-filling) using p-polarised light with an incident angle of 73°. All spectra reported are a ratio of 1000 sample scans to 1000 background scans, the latter recorded for a close-packed monolayer of $TiO_2$ nanocrystals on conducting glass substrate.

**Infrared transmission spectroscopy**

Also recorded were infrared transmission spectra of **I** and **II** in the crystalline state. The final spectra were obtained by co-addition of 100 scans recorded under a nitrogen purge at 1 cm$^{-1}$ resolution for a known concentration of the crystalline compound in a KBr pellet (0.05 mg in 100.00 mg of KBr). The optical path length was determined by measurement of the thickness of the KBr pellet. All spectra reported are a ratio of 100 sample scans to 100 background scans; the latter recorded for a blank KBr pellet of the same thickness.

**Real-time transient optical absorption spectroscopy**

Transient absorption spectra were measured by irradiating the sample with a 5 ns pulse at 355 nm from a Continuum Surelight Nd:YAG laser and using a pulsed Xe-lamp aligned perpendicularly to the beam as a probe source. The 150W Xe-lamp, equipped with an applied photophysics model 408 power supply and applied photophysics model 410 pulsing unit, allowed generation of 0.5 ms pulses. An Oriel model 71445 shutter was placed between the lamp and the sample and was opened for 100 ms to prevent fatigue of the PMT. Bandpass filters, both pre- and post- cut-off, were used to minimise the adverse effects of scattered light. The samples were placed at an angle of 45° with respect to the laser and probe light and set-up in such a way that the scattered light was reflected away from the detector. By doing this, it was possible to record in the early time domain ($t > 50$ ns) without measuring artefacts due to scattered light. Sample rate was kept relatively low (10 s intervals) to prevent electron accumulation in the semiconductor materials. Light was collected in a LDC analytical monochromator, detected by a Hamamatsu R928 Photomultiplier tube and recorded on a Le Croy 9360, 600 MHz oscilloscope. The laser oscillator, Q-switch, lamp, shutter and trigger were externally controlled using a digital logic circuit that allowed for synchronous timing. Absorbance was plotted against time.

In the course of these experiments organised heterosupramolecular assemblies were prepared as described above. Specifically, aqueous electrolyte solutions, containing $LiClO_4$ (0.2 mol dm$^{-3}$) at pH 3 (added perchloric acid) and NaSCN hole scavenger (0.1 mol dm$^{-3}$), were degassed by bubbling with Ar for 30 min. These assemblies formed the working electrode (1 cm$^2$ surface area) of a closed three-electrode single compartment cell, the counter electrode being platinum and the reference electrode a saturated calomel electrode (SCE).

## Acknowledgement

These studies were supported in part by a grant from the Commission of the European Union under the Training and Mobility of Researchers (Network) Programme (Contract FMRX CT96 – 0076).

[1] a) X. Marguerettaz, L. Cusack, D. Fitzmaurice, *Nanoparticle Characterisations and Utilisations* (Ed. J. Fendler), VCH-Wiley, New York, **1998**, Ch. 16; b) S. Connolly, S. N. Rao, R. Rizza, N. Zaccheroni, D. Fitzmaurice, *Coord. Chem. Rev.* **1999**, *185*, 277.
[2] a) J.-M. Lehn, *Supramolecular Chemistry*, VCH, Weinheim, **1995**, Ch. 8; b) V. Balzani, F. Scandola, *Supramolecular Photochemistry*, Ellis Horwood, New York, **1991**, Ch. 3.
[3] a) X. Marguerettaz, R. O'Neill, D. Fitzmaurice, *J. Am. Chem. Soc.* **1994**, *116*, 2628; b) X. Marguerettaz, D. Fitzmaurice, *J. Am. Chem. Soc.* **1994**, *116*, 5017.
[4] a) L. Cusack, S. N. Rao, D. Fitzmaurice, *Chem. Eur. J.* **1997**, *3*, 202; b) L. Cusack, X. Marguerettaz, S. N. Rao, J. Wenger, D. Fitzmaurice, *Chem. Mater.* **1997**, *9*, 1765.
[5] X. Marguerettaz, G. Redmond, S. N. Rao, D. Fitzmaurice, *Chem. Eur. J.* **1996**, *2*, 420.
[6] N. Kotov, F. Meldrum, J. Fendler, *J. Phys. Chem.* **1994**, *98*, 8827.
[7] N. Serpone, D. Lawless, R. Khairutdinov, *J. Phys. Chem.* **1995**, *99*, 16646.
[8] S. Doherty, D. Fitzmaurice, *J. Phys. Chem.* **1996**, *100*, 10732.
[9] a) B. O'Regan, M. Grätzel, D. Fitzmaurice, *Chem. Phys. Lett.* **1991**, *183*, 89; b) G. Rothenberger, D. Fitzmaurice, M. Grätzel, *J. Phys. Chem.* **1992**, *96*, 5983.
[10] J. Pankov, *Optical Processes in Semiconductors* Dover, New York, **1971**, p 74.
[11] a) E. Burstein, *Phys. Rev.* **1969**, *184*, 733; b) T. S. Moss, *J. Appl. Phys.* **1961**, *32*, 2136; c) C. Liu, A. Bard, *J. Phys. Chem.* **1989**, *93*, 7749.
[12] H. Finklea, *Semiconductor Electrodes* Elsevier, New York, **1988**, pp. 65 – 66.
[13] R. Hunter, *Zeta Potential In Colloidal Science* Academic Press, London, **1981**.
[14] J. Woodward, A. Ulman, D. Schwartz, *Langmuir* **1996**, *12*, 3626.
[15] W. Siripala, M. Tomkievicz, *J. Electrochem. Soc.* **1982**, *129*, 1240.
[16] a) H. Frei, D. Fitzmaurice, M. Grätzel, *Langmuir* **1990**, *6*, 198; b) J. Moser, S. Punchihewa, P. Infelta, M. Grätzel, *Langmuir* **1991**, *7*, 3012; c) P. Pechy, F. Rotzinger, M. K. Nazeeruddin, O. Kohle, S. M. Zakeeruddin, R. Humphry-Baker, M. Grätzel, *J. Chem. Soc. Chem. Comm.* **1995**, 65.
[17] *Langmuir-Blodgett Films* (Ed. G. Roberts), Plenum, New York, **1990**.
[18] a) Y. Obeng, A. Founta, A. Bard, *New J. Chem.* **1992**, *16*, 121; b) T. Nagamura, Y. Isoda, K. Sakai, T. Ogawa, *J. Chem. Soc. Chem. Commun.* **1990**, 703; c) M. Schmezler, M. Burghard, P. Bäuerle, S. Roth, *Thin Solid Films* **1994**, *243*, 620.

  0947-6539/01/0706-1320 $ 17.50+.50/0 

[19] a) B. Kok, H. Rurainski, O. Owens, *Biochem. Biophys. Acta* **1965**, *109*, 347; b) P. Trudinger, *Ananl. Biochem.* **1970**, *36*, 222; c) T. Wantanabe, K. Honda, *J. Phys. Chem.* **1982**, *86*, 2617.
[20] N. Gershfeld, *Annu. Rev. Phys. Chem.* **1976**, *27*, 349.
[21] X. Marguerettaz, D. Fitzmaurice, *Langmuir* **1997**, *13*, 6769.
[22] a) D. Allara, R. Nuzzo, *Langmuir* **1985**, *1*, 52; b) A. Parikh, D. Allara, *J. Chem. Phys.* **1992**, *96*, 927.
[23] In undertaking these simulations the measured spectra were normalised with respect to the effective surface concentration of alkyl chain in the close-packed monolayer in $TiO_2$(1)-**B**.

Received: October 7, 1999
Revised version: October 5, 2000 [F2072]